Journal of Quantitative Spectroscopy & Radiative Transfer 206 (2018) 392–398

Contents lists available at ScienceDirect

Journal of Quantitative Spectroscopy & Radiative Transfer

journal homepage: www.elsevier.com/locate/jqsrt

UV–Vis–IR spectral complex refractive indices and optical properties of brown carbon aerosol from biomass burning

Benjamin J. Sumlin[a,1], Yuli W. Heinson[a,1], Nishit Shetty[a], Apoorva Pandey[a], Robert S. Pattison[b], Stephen Baker[c], Wei Min Hao[c], Rajan K. Chakrabarty[a,*]

[a] Center for Aerosol Science and Engineering, Department of Energy, Environmental and Chemical Engineering, Washington University in St. Louis, St. Louis, MO 63130, USA
[b] United States Forest Service, Pacific Northwest Research Station, Anchorage, AK 99501 USA
[c] Missoula Fire Sciences Laboratory, United States Forest Service, Missoula, MT 59808 USA

ARTICLE INFO

Article history:
Received 6 October 2017
Revised 13 December 2017
Accepted 13 December 2017
Available online 15 December 2017

Keywords:
Brown carbon aerosol
Complex refractive index
Optical properties

ABSTRACT

Constraining the complex refractive indices, optical properties and size of brown carbon (BrC) aerosols is a vital endeavor for improving climate models and satellite retrieval algorithms. Smoldering wildfires are the largest source of primary BrC, and fuel parameters such as moisture content, source depth, geographic origin, and fuel packing density could influence the properties of the emitted aerosol. We measured *in situ* spectral (375–1047 nm) optical properties of BrC aerosols emitted from smoldering combustion of Boreal and Indonesian peatlands across a range of these fuel parameters. Inverse Lorenz–Mie algorithms used these optical measurements along with simultaneously measured particle size distributions to retrieve the aerosol complex refractive indices ($m = n + i\kappa$). Our results show that the real part n is constrained between 1.5 and 1.7 with no obvious functionality in wavelength (λ), moisture content, source depth, or geographic origin. With increasing λ from 375 to 532 nm, κ decreased from 0.014 to 0.003, with corresponding increase in single scattering albedo (SSA) from 0.93 to 0.99. The spectral variability of κ follows the Kramers-Kronig dispersion relation for a damped harmonic oscillator. For $\lambda \geq 532$ nm, both κ and SSA showed no spectral dependency. We discuss differences between this study and previous work. The imaginary part κ was sensitive to changes in FPD, and we hypothesize mechanisms that might help explain this observation.

1. Introduction

Organic aerosols (OA) account for a large fraction of the total tropospheric particulate matter burden [1,2]. These aerosols have been typically considered to predominantly scatter light in the visible solar spectrum. However, findings from field [3,4] and laboratory studies [5,6] show that a class of OA, optically defined as brown carbon (BrC), significantly absorb in the shorter visible wavelengths ($\lambda \sim 350$–550 nm) with absorption Ångström exponents (AAE) ranging between 2 and 12 [7]. BrC aerosols have physical, chemical, and optical properties distinct from black carbon (BC) aerosols. BC has a fractal-like morphology with a deep black appearance caused by a significant, non-zero imaginary part κ of its complex refractive index (RI) that is wavelength-independent over the visible and near-visible wavelengths [8]. In contrast, BrC aerosols are spherical in morphology and are yellow-brown in color due to values of κ that increase sharply toward shorter visible and ultraviolet wavelengths. Constraining and parameterizing the spectral optical properties and RIs of BrC aerosols across the solar spectrum has been a challenging endeavor for the atmospheric aerosol community. Climate models and satellite retrieval algorithms rely on this information for accurate retrievals and predictions of aerosol optical depths.

Primary BrC aerosol emissions are largely attributed to biomass and biofuel burning [9–11] and biogenic release of soil and humic matter [7,12]. In particular, it is the smoldering phase of biomass burning that has been identified as the major source of these particles [10,13,14]. Recent studies show that boreal and Indonesian peat fires are the largest contributors of primary BrC aerosols to regional emissions, and contribute up to 72% of all carbon emissions in a given year [15]. Peatlands store between one-fifth and one-third of earth's organic carbon and act as a net carbon sink, but this carbon is increasingly released back to the atmosphere since peatlands face an increasing threat of wildfires due to rising global temperatures [16–18]. Peat fires are dominated by smolder-

* Corresponding author.
E-mail address: chakrabarty@wustl.edu (R.K. Chakrabarty).
[1] These authors contributed equally to this work.

https://doi.org/10.1016/j.jqsrt.2017.12.009
0022-4073/

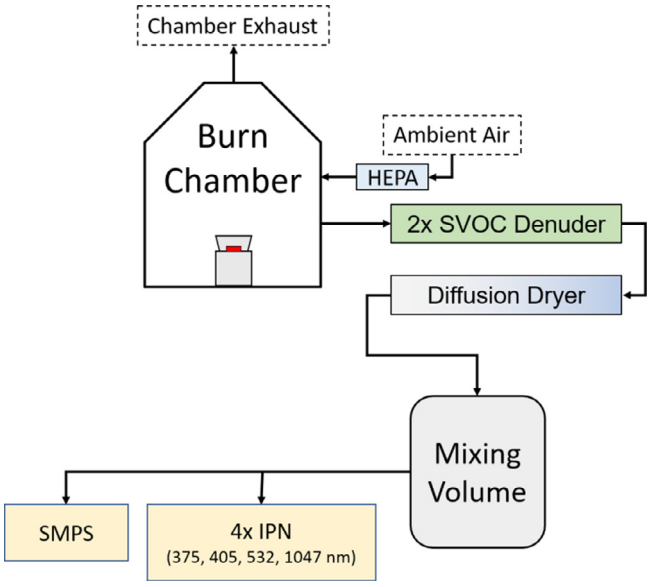

Fig. 1. A schematic diagram of the experimental setup showing the SVOC denuders, diffusion dryer, mixing volume barrel, SMPS, and IPNs.

ing phase combustion which can persist in low to moderate fuel moisture conditions, and is capable of lasting for several weeks or longer [19].

In this study, we present our results from *in situ,* contact-free measurements of spectral (UV–Vis–IR) optical properties and size distributions of BrC aerosol emitted from laboratory-scale smoldering combustion of peat samples collected from different parts of Alaska and Indonesia. Scattering and absorption coefficients β_{sca} and β_{abs} were measured using four integrated photoacoustic-nephelometers (IPNs). In conjunction with size distribution measurements by a scanning mobility particle sizer (SMPS, TSI, Inc., Shoreview, MN), these optical measurements were inverted using Mie theory for the retrieval of complex RIs ($m = n + i\kappa$). Best efforts were made to mimic real-world smoldering fire scenarios in our laboratory experiments. Smoldering fire behavior fluctuates across a typical forest floor because of spatial variability in fuel depth, fuel packing density (FPD, mass per unit volume), mineral content, and moisture content (MC) [20–26]. The probability that peat will burn and sustain once ignited depends heavily on MC and FPD. We studied the variation in optical properties and size distributions of emitted smoke aerosols as a function of varying fuel depths, FPDs, and MCs. When compared to previous studies, we find that FPD has the strongest effect on BrC absorption properties, with κ varying directly with FPD. Finally, we constrain previous literature results and our experimental findings on $\kappa(\lambda)$ using the analytical form of the Kramers–Kronig dispersion relation for a damped harmonic oscillator [27].

2. Experimental methods

Fig. 1 shows the schematic diagram of our experimental setup. The setup consists of a sealed 21 m^3 stainless steel chamber equipped with a computer-controlled ignition system and a recirculation fan. The ignition system is a 1 kW ring heater (McMaster-Carr 2927094A) coupled to a 1/16″ stainless steel plate, and its temperature is monitored by a K-type thermocouple to close the control loop. We studied peat samples collected from Alaska (AK) and Indonesia (IN). The AK peat samples were separated into collection depths of 0–4″ and 4–8″ below the surface from sites dominated by sphagnum and black spruce (*Picea mariana*). Typically, canopy cover of black spruce was about 40%. The understory was typically sparse, with species such as dwarf birch (*Betula nana*) and varieties of *Rhododendron* subsect. *Ledum, Vaccinium* and *Empetrum*. The AK peat samples were naturally dried to 5%, 10%, 15%, 20%, and 40% MC at room temperature. The IN peat samples were not depth-resolved and were dried to 5%, 20%, and 40% MCs. IN forest speciation information was unavailable due to the high degree of biodiversity in southeast Asian rainforests. Approximately 2 g of each fuel sample was placed on the heating plate such that the FPD was ~0.03 g/cm^3, and smoldering was initiated by heating the plate to 245 °C. One hour after ignition, aerosols were sampled from ports approximately 2 m above the chamber floor. Gas-phase products were removed with activated parallel-plate semivolatile organic carbon (SVOC) denuders (Sunset Laboratory, Inc., Tigard, OR), and excess water was removed with a diffusion dryer packed with indicating silica beads (McMaster-Carr 2181K97). Finally, the aerosols were mixed in a 208 liter barrel (McMaster-Carr 4392T47) and a homogeneous, isokinetic stream was sampled by each IPN and the SMPS.

The IPNs used in this study are of our own design and construction, and are briefly described in the Supporting Material. We operated four IPNs at $\lambda = 375$, 405, 532, and 1047 nm. The IPNs measured β_{sca} and β_{abs} continuously with 2 sec time resolution, from which the single scattering albedo (SSA) was calculated. The SMPS measured particle number size distributions every 5 min. IPN measurements were averaged over 5 min to align with the SMPS measurement intervals.

Complex RI was retrieved using PyMieScatt, a Lorenz–Mie theory package for Python 3 [28]. PyMieScatt includes inversion functions that take measurements of β_{abs}, β_{sca}, and the size distribution to return m. The theory behind the retrieval algorithms is detailed in [26]. To minimize computing overhead, we chose PyMieScatt's Survey-Iteration algorithm. Briefly, this is a two-stage algorithm that first constructs coarse arrays of $\beta_{abs}(n,\kappa)$ and $\beta_{sca}(n,\kappa)$ for a given size distribution and wavelength of light, and surveys them for values that are close to the IPN measurements. Values with array indices that are common to both the β_{abs} (n,κ) and β_{sca} (n,κ) arrays are considered candidate solutions. The iteration stage is best described by Fig. 2. The real part of the refractive index is treated first in the red "Scattering" loop, and then the imaginary part is treated by the blue "Absorption" loop. The algorithm runs for each candidate m found by the survey. When a solution is found, the algorithm reports m along with E_{abs} and E_{sca}, which are the residuals between simulated and measured β_{abs} and β_{sca}.

We report n and κ as the average of twelve individual retrievals performed in 5-minute data intervals over an hour. Uncertainties for n, κ, SSA, AAE, and κ Ångström exponent (κAE) are propagated through the retrievals and we report the overall standard deviation using

$$\sigma_{\text{overall}} = \sqrt{\frac{\sum_i^N \sigma_i^2}{N}}, \quad (1)$$

where σ_i is the standard deviation of each data point and N is the total number of data points.

3. Results and discussion

In this section, we refer to AK peat samples by their MCs and source depths. The IN samples are labeled according to their MCs. Tabulated data of all graphs and SMPS size distribution plots can be found in the Supporting Material.

3.1. Complex refractive indices

The spectral dependence of m is plotted in Fig. 3. For both AK and IN peat, n is constrained between 1.5 and 1.7, and the spread of data belies any obvious trend in λ. However, we note that n